Semiconductor Physics, Quantum Electronics & Optoelectronics, 2013. V. 16, N 4. P. 322-330.

PACS 68.37.Ps, 78.67.Wj

Graphene layers fabricated from the Ni/a-SiC bilayer precursor

A.N. Nazarov[1,2], A.V. Vasin[1], S.O. Gordienko[1], P.M. Lytvyn[1], V.V. Strelchuk[1], A.S. Nikolenko[1], Yu.Yu. Stubrov[1], A.S. Hirov[2], A.V. Rusavsky[1], V.P. Popov[3], V.S. Lysenko[1]
[1]*V. Lashkaryov Institute of Semiconductor Physics, National Academy of Sciences of Ukraine, 45, prosp. Nauky, 03028 Kyiv, Ukraine*
[2]*National Aviation University, Department of Theoretical and Applied Physics, Kyiv, Ukraine*
[3]*A.V. Rzhanov Institute of Semiconductor Physics, Russian Academy of Sciences, Novosibirsk, Russia*
Phone/fax:+38 (044) 525-61-77; e-mail: nazarov@lab15.kiev.ua

Abstract. This paper considers a synthesis of graphene flakes on the Ni surface by vacuum long and nitrogen rapid thermal treatment of the "sandwich" amorphous (a) SiC/Ni multilayer deposited on silicon wafer by magnetron sputtering technique. The lateral size of graphene flakes was estimated to be about hundreds of micrometers while the thickness estimated using Raman scattering varied from one to few layers in case of vacuum annealing. Rapid thermal annealing (RTA) in nitrogen ambient results in formation of multilayer graphene with surface covering up to 80%. The graphene layers synthesized on Ni during CVD process was used as reference samples. Atomic force microscopy (AFM) is not able to detect graphene flakes in regime of surface topology examination because of large roughness of Ni surface. Employment of scanning Kelvin probe force microscopy (SKPFM) demonstrates correlation of the surface potential and graphene flakes visible in optical microscopy. Using the KPFM method, potential differences between Ni and graphene were determined.

Keywords: graphene, a-SiC, magnetron sputtering, micro-Raman, AFM, scanning Kelvin probe force microscopy.

Manuscript received 15.07.13; revised version received 18.09.13; accepted for publication 23.10.13; published online 16.12.13.

1. Introduction

In the article [1], the original simple method to synthesize graphene layers from solid source was suggested. As a solid carbon source, the amorphous a – Si produced by chemical vapor deposition (CVD) on SiO_2-Si wafer and covered with a Ni layer was used. The method allowed to synthesize enough large graphene areas and employed shorter heating time as compared with thermal decomposition of crystalline SiC [2]. In this paper, the a – Si layer was proposed to be deposited by RF magnetron technique and the Ni layer by DC magnetron technique without removal of the wafer from the chamber. The article focuses attention on study of graphene synthesis in such a system by using annealing in different ambience (vacuum and nitrogen) and different times (short – 5 s and long – 20 min), and comparison of optical and structural properties of the fabricated graphene with commercial graphene layers deposited by the CVD method [3].

2. Experimental details

2.1. Sample fabrication

The graphene layers were synthesized by vacuum thermal treatment at 700…900 °C for 2 to 20 min and by rapid thermal annealing (RTA) in ambient nitrogen at temperatures 800…900 °C for 5 to 30 s of the sandwich a – $Si_{1-x}C_x$/Ni structure deposited on SiO_2 film with the thickness close to 200 nm (see Fig. 1a). The a – $Si_{1-x}C_x$ was deposited on oxidized Si wafer by RF magnetron sputtering the polycrystalline SiC target in Ar, and the Ni film by DC magnetron sputtering the Ni target without removal of the wafer from the chamber. The

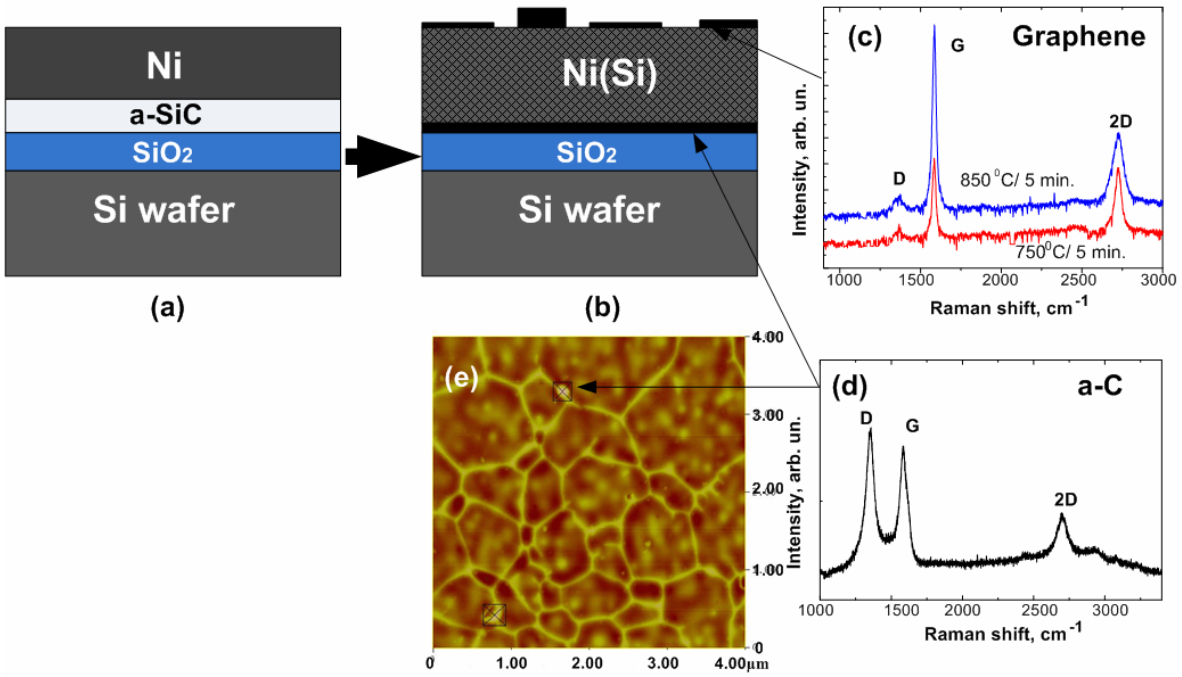

Fig. 1. Diargam of the structure transformation after high-temperature annealing of Ni/a-SiC/SiO_2/Si structure: before annealing (a); after annealing (b). Raman spectra of graphene synthesized on the Ni(Si) surface (c); Raman spectra (d) and AFM image (e) of a-C synthesized on the SiO_2 surface.

thickness of the $a-Si_{1-x}C_x$ layer was estimated using AFM measurements as 50 nm and thickness of the Ni layer – 500 nm. For comparison, we used graphene films deposited by CVD methods at 900 °C for 20 min on Ni layer covering the SiO_2-Si wafer.

2.2. Measurement techniques

The $a-Si_{1-x}C_x$ film chemical composition and local structure were analyzed using Auger-electron spectroscopy (AES; Jump 10s, JEOL), Fourier-transform infra-red spectroscopy (FTIR; 2000FT-IR, Perkin–Elmer) and micro-Raman spectroscopy (mRS, triple Raman spectrometer T-64000 Horiba Jobin-Yvon, equipped with electrically cooled CCD detector, and excitation by the 514 nm line of an Ar-Kr ion laser). The surface morphology of the nickel layer after thermal annealing was studied by Scanning Electron Microscopy (SEM). The graphene surface morphology and distribution of electrical potential were studied by optical microscopy (Axioscop 2 MAT, Carl Zeiss) in standard and differential interference contrast (DIC) mode, AFM and scanning Kelvin probe force microscopy (SKPFM, NanoScope IIIa Dimension 3000).

The surface morphology and surface potential map were measured using two-path technique. For this technique, firstly, a map of surface was obtained, and, secondly, the probe was lifted up to some height (in our case the lift height was 100 nm), and the electrostatic surface potential map was measured using the Kelvin probe technique. For the SKPFM method, Si probe (EFM 20, NanoWorld) covered with Pt/Ir film was used, and applied ac voltage V_{ac} was 3 V.

The SKPFM method allowed us to obtain clear contrast from phase inhomogeneity surfaces by measuring the local potential contact difference V_{dc} between scanning microscopy tip V_{tip} and surface under the tip V_{surf} [4]. To measure this contact potential difference, the ac voltage $V_{ac}\cos\omega t$ was applied to the tip, which generated electrostatic field F oscillating with the frequency ω:

$$F = (dC/dz)V_{dc}V_{ac}, \qquad (1)$$

where dC/dz is the deriviative of the tip-surface capacitance at the height and $V_{dc} = V_{tip} - V_{surf}$. The electrostatic field equals zero, if the tip potential equals to the surface one ($V_{tip} = V_{surf}$). Thus, in the SKPFM method the tip potential is chosen by the feedback system in such a manner that the electrostatic field F equals zero.

3. Results and discussion

3.1. Chemical composition of the as-deposited a-$Si_{1-x}C_x$ layer

The chemical composition of the as-deposited $a-Si_{1-x}C_x$ film was analyzed using Auger electron spectroscopy with the relative sensitivity factors of C(KVV) and

Si(LVV) lines obtained from the bulk crystalline 6H–SiC standard. Silicon-to-carbon ratio was estimated to be about 40/60.

Within the range of 500 – 3000 cm^{-1}, the FTIR transmission spectra of as-deposited samples showed one pronounced band near 760 cm^{-1} (Si–C stretching mode) typical for a-SiC layers [5]. The IR bands associated with hydrogen bonds were not observed.

The Raman spectrum demonstrated very broad band centered around 1489 cm^{-1}. This band should be attributed to amorphous carbon clusters. Usually Raman scattering spectra of amorphous carbon are represented by a superposition of two bands, the so-called *G* band (graphitic, 1500 – 1600 cm^{-1}) and *D* band (disordered, 1300 – 1400 cm^{-1}), that are manifestations of a disordered graphite-like (sp^2-coordinated) structure. It is generally recognized that the ratio of intensities of *D* and *G* bands (I_D/I_G) depends on the carbon cluster size. For a cluster size larger than 1.2…2.5 nm, the I_D/I_G ratio decreases as cluster becomes larger. But for crystallites smaller than 1.2…2.5 nm, the smaller the cluster size the smaller is the ratio I_D/I_G [6]. The broad single RS band that we observed in as-deposited a-SiC films is quite unusual. We do not discuss here peculiarity of RS band but attribute it to very small (smaller than 2 nm) and highly disordered amorphous carbon clusters. Evolution of this band with annealing was studied in details elsewhere [7].

Thus, our as-deposited a – $Si_{1-x}C_x$ layer is carbon-enriched amorphous SiC with small (smaller than 2 nm) carbon amorphous nanoclusters inside this material.

3.2. Surface morphology of the Ni/a-$Si_{1-x}C_x$/SiO_2/Si structures: SEM and optical microscopy

Measurements of SEM show that surface of as-deposited Ni layer on a – $Si_{1-x}C_x$ film has a nanograin structure with the size of nanograins not larger than 50 nm (Fig. 2a). After vacuum annealing at 800 °C, the Ni layer is crystallized with the size of crystallites close to 1…0.5 μm (Fig. 2b), and after 1150 °C the size of Ni grains reaches up to 2 μm (Fig. 2d). Thus, due to formation of the Ni micrograines after high-temperature annealing, for enhancement of the surface flatness we have to decrease the annealing temperature and time of graphene layer formation.

Standard optical microscopy images of the Ni surface after vacuum annealing at 800 °C for 2 to 30 min are presented in Fig. 3. It can be seen that thin and thick graphene flakes are located on Ni surface with the size of thin flakes larger than 20 μm. Increase in time of vacuum annealing results in an increased amount of

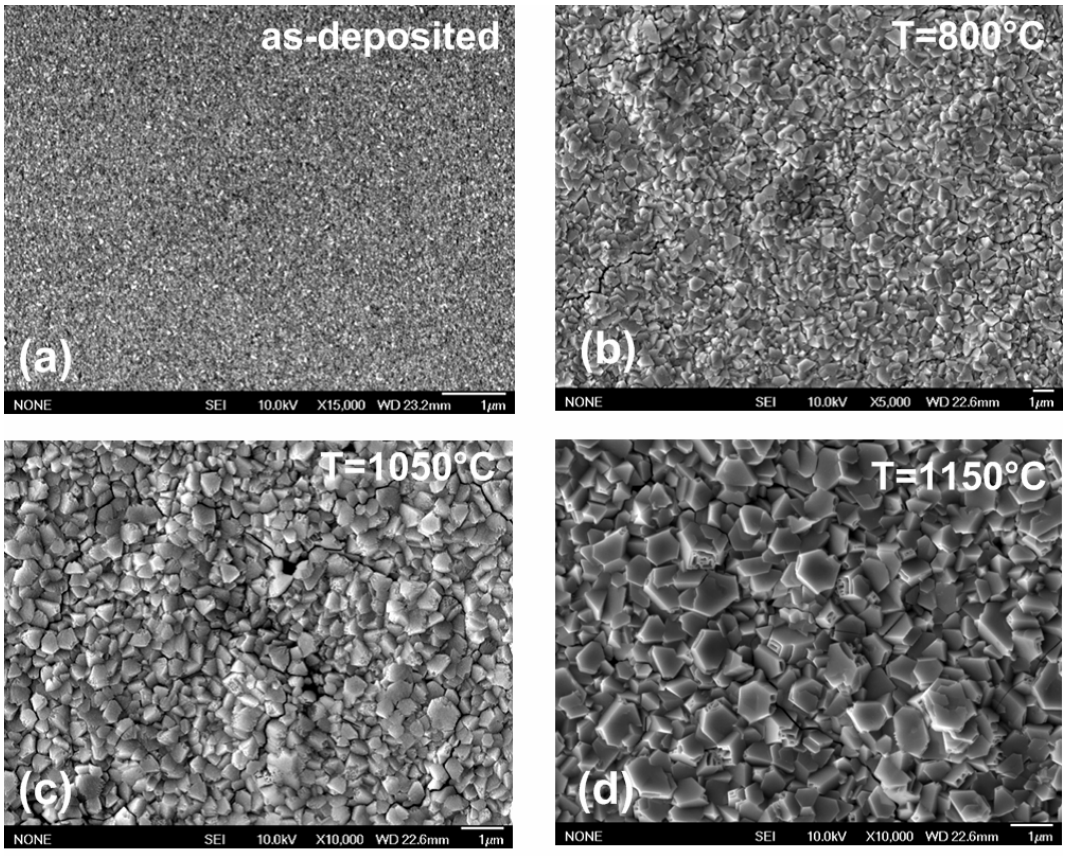

Fig. 2. The SEM pictures of Ni surface as-deposited on a-SiC layers (a) and after high-temperature thermal annealing in vacuum for 5 minute at temperature 800°C (b), 1050°C (c) and 1150°C (d).

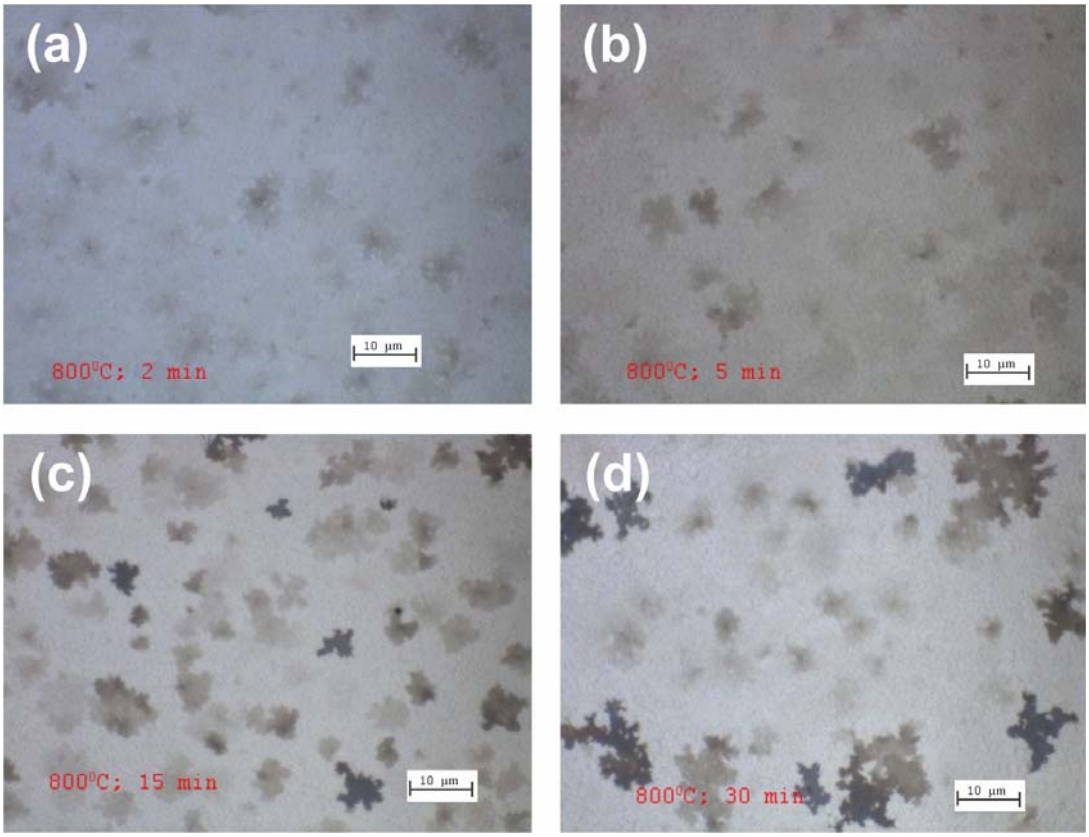

Fig. 3. Standard optical microscopy mode measurement of graphene flaked on Ni after vacuum annealing at 800°C for: 2 min (a), 5 min (b), 15 min (c) and 30 min (d).

multilayer graphene flakes. Measurements in DIC mode demonstrate a microcrystalline structure of Ni surface with the size of Ni grains close to 1 μm (Fig. 4b). Thus, the graphene flakes cover large areas of polycrystalline Ni surface.

Fig. 4 demonstrates comparison of the optical microscopy imagies of the Ni surfaces with graphene flakes synthesized using the solid source ($a - Si_{1-x}C_x$) and CVD technique. In case of the CVD technique, we observed more full graphene covering of the Ni surface than in the case of graphene synthesis from the solid source after vacuum annealing, however, the Ni surface in the latter case is less structured (Figs 4b and 4d), which indicates lower used temperatures and times for graphene synthesis from the solid source.

After RTA in ambient nitrogen at the temperature 850 °C of the Ni/$a - Si_{1-x}C_x/SiO_2$/Si structure, graphene covering of the Ni surface reaches up to 90% (Fig. 5). Increase of the treatment time results in increase of the layer thickness.

3.3. Raman spectroscopy measurements

In Figs 1c and 1d, Raman spectra measured on the Ni surface and on the SiO_2 surface after etching of the Ni(Si) layer are presented for the case of the Ni/$a - Si_{1-x}C_x/SiO_2$/Si structure high-temperature annealed in vacuum. In this case, it was integral measurements of the Raman spectrum because of the diameter of excitation light beam was near 100 μm. It can be seen that the Raman spectrum measured on the Ni surface (Fig. 1c) demonstrates appearance of the narrow *G* band (~1600 cm^{-1}), that is indication on the hexagonal graphene lattice formation [6], and clearly pronounced 2*D* band (~2700 cm^{-1}), which originates from a two-phonon double resonance Raman process [8]. Increase in the number of graphene layers results in changing the shape, width and frequency location of the 2*D* band. It's known that generaly in graphite-like materials the 2*D* band intensity is lower than the intensity of *G* band, but the intensity of these bands is identical, when the graphene layer width is less than 5 atomic layers [9]. In our case, we observed the same intensity of *G* and 2*D* band that corresponds to the graphene layer on Ni surface with the thickness close to 5 atomic layers. Presence of the *D* band (~1335 cm^{-1}) of a low intensity proves appearance of defects in the graphene layers [8]. At the same time, the Raman spectrum measured on the SiO_2 surface manifests the *G* and *D* bands with equal intensities and the 2*D* band with a very small intensity of the signal (Fig. 1d). Such Raman spectrum can be associated with strongly damaged graphite [10]. AFM

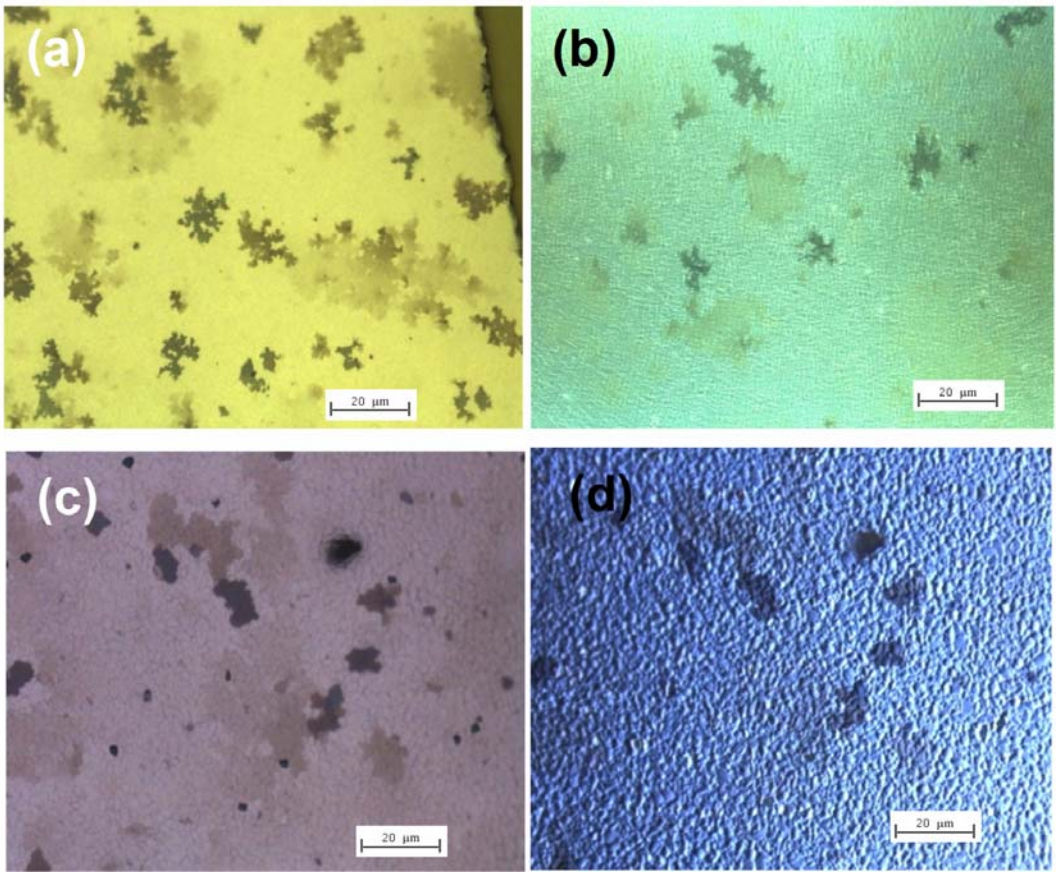

Fig. 4. Standard (a, c) and Differential Interference Contrast (DIC) (b, d) optical microscopy mode measurement of graphene flaked on Ni after vacuum annealing at 800°C for 5 min (a, b) and CVD deposited at 900°C for 20 min (c, d). All pictures have the same scale.

image of this surface is presented in Fig. 1e. It looks like replica of the crystalline Ni layer on carbon layer (see Figs 2b and 2c).

Using micro-Raman spectroscopy to study properties of graphene flakes with different thicknesses synthesized on Ni surface after vacuum annealing is presented in Fig. 6. The number of atomic graphene layers can be estimated using the ratio of intensities I_G/I_{2D} and also by half-width of 2*D* band [8]. In the case presented in Fig. 6, when $I_G/I_{2D} \approx 0.30$, the number of graphene layers can correspond to unity. Increase in the number of graphene layers leads to growth of the I_G/I_{2D} ratio, and the half-width of 2*D* band changes from 33 to 75 cm^{-1}. In spite of the half-width broadening at transition from single layer to the triple one, the shape of 2*D* band is well described by a single Lorentz curve. At the same time, the position and half-width of *G* band remains almost the same. The similar phenomenon is observed also for graphene layer epitaxially synthesized on SiC [11]. Absence of thin structure in the 2*D* band at transition from a single-layer to double- and triple-layer graphene can be associated with changing of electron band structure related with reduction of interaction between graphene layers. Thus, in the Raman spectra of disoriented double layer graphene the 2*D* band intensity is higher than that of *G* band, however, the 2*D* band shape is described by one Lorentz curve similarly to single-layer graphene, and its frequency position shifts to higher frequencies [12, 13].

Comparison of Raman spectra measured in single-layer graphene synthesized using our technique and in mechanically exfoliated graphene [14] is presented in Fig. 7a. In the Raman spectrum of graphene synthesized from the solid source, 2*D* band at 2722.4 cm^{-1} and with the half-width 33 cm^{-1} is observed, the latter being shifted to the high-frequency side by $\Delta\omega \approx 33$ cm^{-1} in comparison with 2*D* band in exfoliated graphene. The half-width of the 2*D* band in exfoliated graphene is 20 cm^{-1}. At the same time, the shift of *G* band in graphene synthesized from the solid source as compared with that of exfoliated graphene is only $\Delta\omega \approx 2$ cm^{-1} (from 1582.3 up to 1584.2 cm^{-1}), but the half-width of *G* band is wider (18 cm^{-1}) than that in exfoliated graphene (9 cm^{-1}). *G* and 2*D* band widening for the synthesized graphene is usually associated with inhomogeneous residual strains that are generated during cooling the

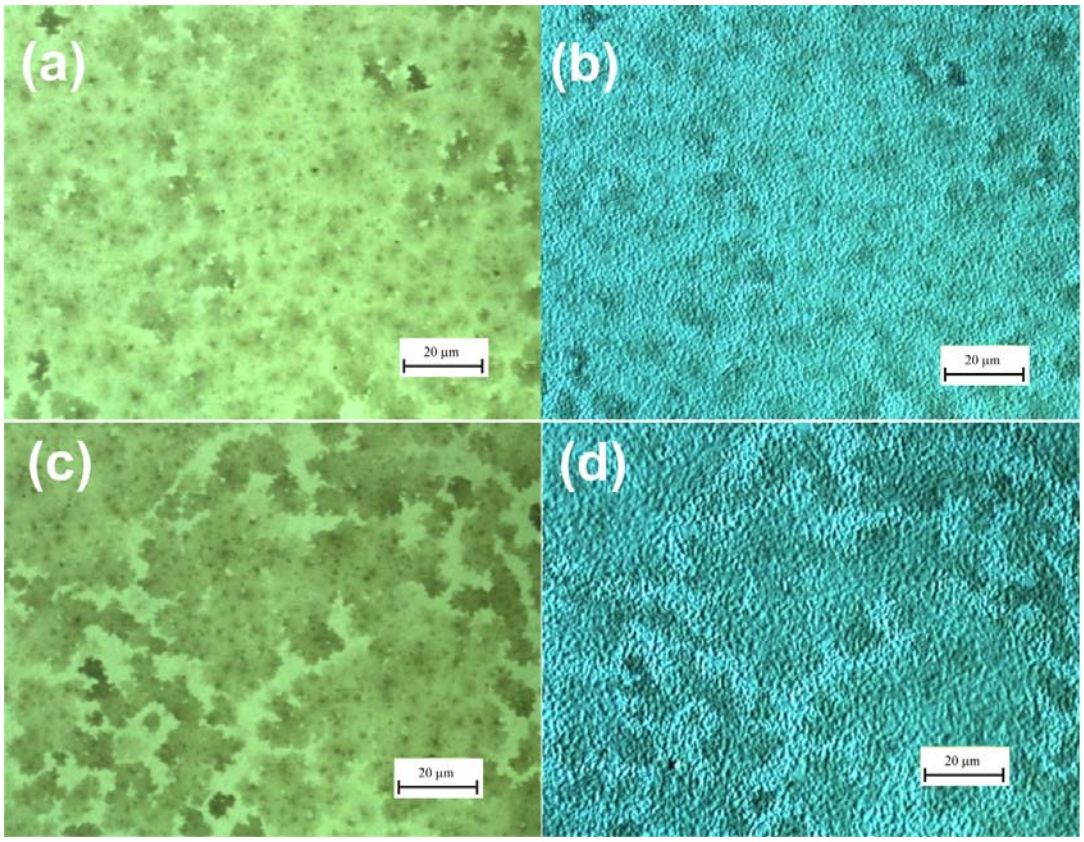

Fig. 5. Standard (a, c) and Differential Interference Contrast (DIC) (b, d) optical microscopy mode measurement of graphene flaked on Ni after RTA at 850°C for 30 s (a, b) and 90 s (c, d).

material [1, 15] or structural inhomogeneities related with deviation of the graphene layers from planarity [16].

It should be noted that the studied graphene layers can possess a space inhomogeneous distribution of double- and multilayer graphene fragments that can lead to widening the 2*D* band due to averaging the Raman signal in a region with diameter of 1 μm [16]. However, in our case the ratio I_{2D}/I_G is significant and the above phenomenon can not be the main factor that causes the 2*D* band widening.

The significant shift of 2*D* band in Raman spectra of the graphene layers epitaxially synthesized on SiC substrate is associated with biaxial compression deformations [17]. If we suggest that in our case the high frequency shift of 2*D* band ($\Delta\omega \approx 30$ cm^{-1}) is caused by compression deformation, the high-frequency shift of *G* band has to be close to $\Delta\omega \approx 8$ cm^{-1}, that is not experimentally observed ($\Delta\omega_{exp} \le 2$ cm^{-1}) [18]. Alternative mechanisms of 2*D* band shifting at almost invariable *G*-band position can be changing the electron band slope around *K* point of the graphene Brillouin zone. Under conditions of double electron-phonon resonance, the above mentioned situation results in shifting the phonon wavevector and correspondingly results in 2*D*-band shifting [19]. Changing the electron band configuration in our case can be associated with either disorientation or inner disorder in graphene layer induced by Ni surface curvature. This hypothesis is supported by existence of defect bands (*D* and D') at high intensity and uniformity of 2*D* band (see Fig. 7a).

To clarify mechanisms of 2*D*-band high-frequency shifting, measurements of Raman spectra with variation in the excitation energy were performed (Fig. 7b). As it can be seen in inset to Fig. 7b dispersion of the 2*D*-band frequency position in our synthesized graphene flakes is linear but with the slope a little sharper than that for single-layer mechanically exfoliated graphene, which indicates electron band slope decrease in the vicinity of *K* point and, hence, decrease of the Fermi velocity in the studied graphene.

Micro-Raman spectra measured on CVD synthesized graphene flakes are presented in Fig. 8a. Positions of *G* band and 2*D* band are very similar to those observed for synthesized from the solid a – $Si_{1-x}C_x$ source and, correspondingly, are 1584 and 2721.6 cm^{-1}. The *D* band at 1335 cm^{-1} is not observed in such samples that demonstrate better structural properties of the CVD synthesized graphene flakes. However, the ratio of intensities I_G/I_{2D} even for very light area is close to 2.3, which corresponds to multilayer (more than 10 atomic layers) graphite.

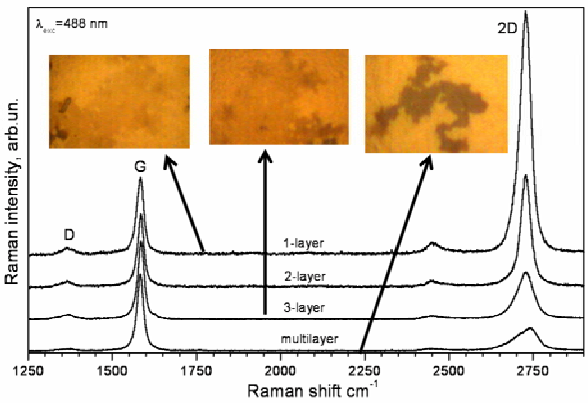

Fig. 6. Comparative micro-Raman spectra for graphene flakes with different number of layers. Insets: Optical microscopy images corresponding to measurement areas.

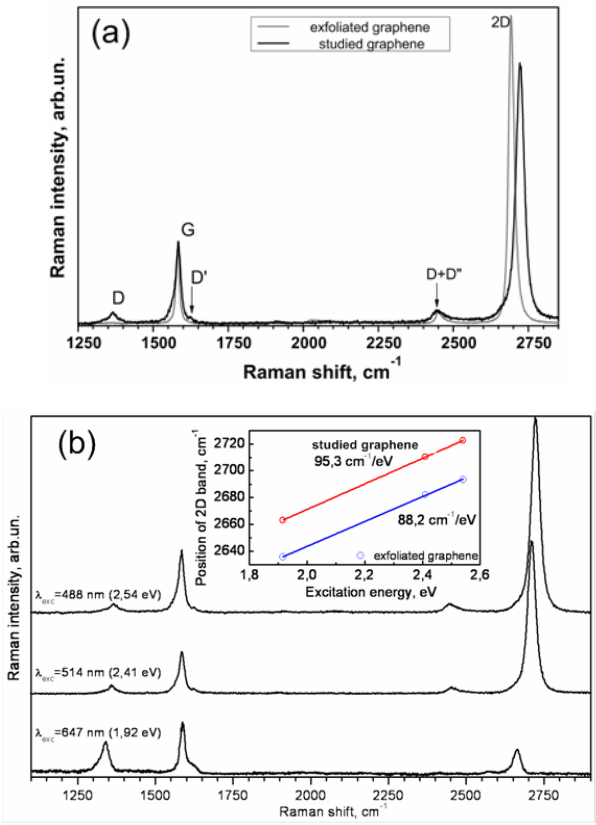

Fig. 7. Comparison of micro-Raman spectra (excitation at 488 nm) for single layer exfoliated graphene and graphene flakes synthesized from solid source (a) and for different excitation wavelengths (b).

The RTA treatment of the Ni/a – $Si_{1-x}C_x/SiO_2/Si$ structures in ambient nitrogen results in good covering the Ni surface by graphene layer (see Fig. 5), but the layer is considerably thicker than in the case of vacuum annealing and very similar to CVD deposited graphene (see Fig. 8b).

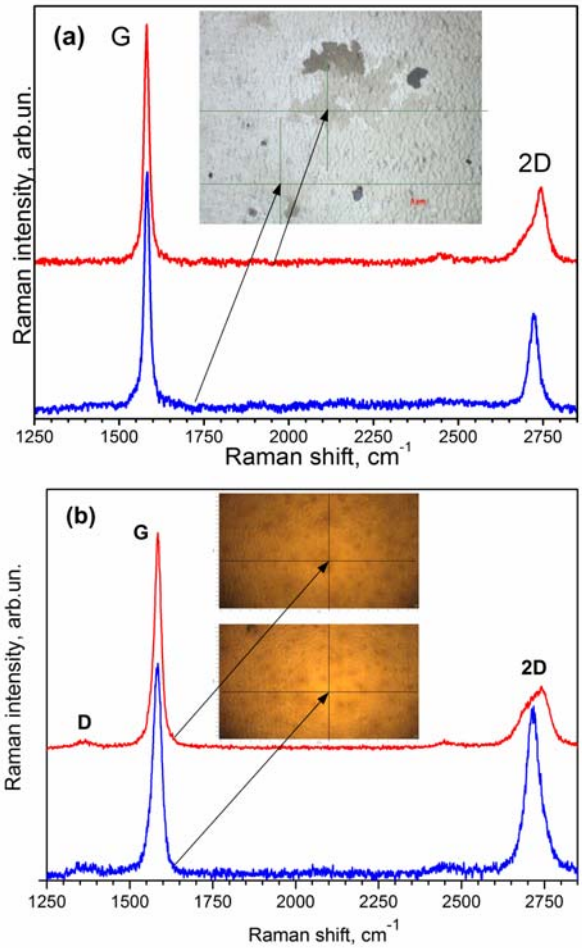

Fig. 8. Micro-Raman spectra for graphene flakes synthesized by CVD technique (a) and from solid source with RTA at 850°C for 30 s in nitrogen ambient (b). Excitation wavelength is 488 nm. Insets: Optical microscopy images corresponding to measurement areas.

3.4. Atomic force microscopy and scanning Kelvin probe force microscopy

AFM image of the Ni surface area with graphene layer after vacuum annealing at 850 °C for 5 min is depicted in Fig. 9a. The Ni film has a microcrystalline structure with the average grain size 1.1±0.5 μm. The surface roughness is 17.5 nm. In the AFM map a graphene flake position is very difficult to extract even in the case of good optical contrast (Fig. 9e). However, due to considerable difference of work functions for Ni and C (5.04–5.35 eV and 4.7–5.1 eV, correspondingly [20]), the graphene flakes demonstrate precise contrast on the surface potential map (Figs 9b and 9c). Combination of the AFM map with the SKPFM one for the same region shows that graphene layer covers closely the Ni grains (Figs 10a and 10b). The surface potential difference between graphene and Ni was determined by SKPFM and is equal to 82 mV (Fig. 9d) that is in good agreement with the work function values in these materials.

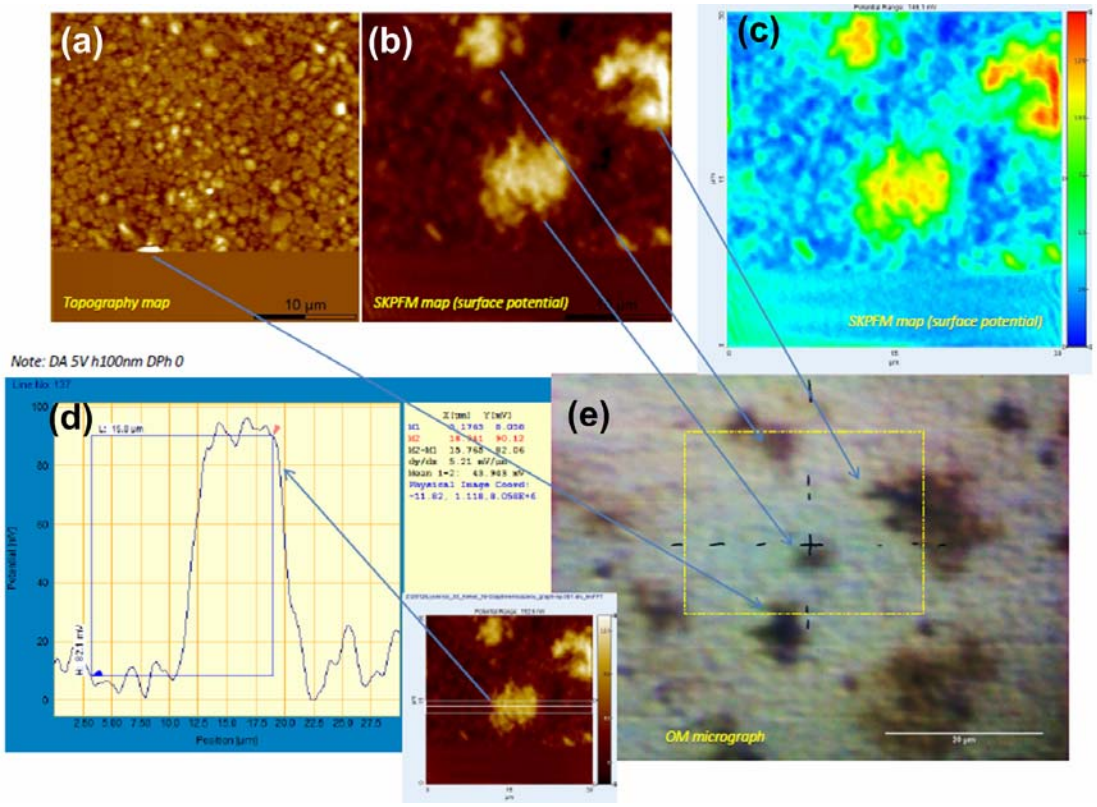

Fig. 9. AFM surface topography map (a), corresponding map of surface potential (b, c) of the surface fragment of the graphene/Ni structure after vacuum annealing at 800°C for 5 min, which optical image is depicted in (e), and surface potential along the line indicated by inset (width of the line corresponds to area of average).

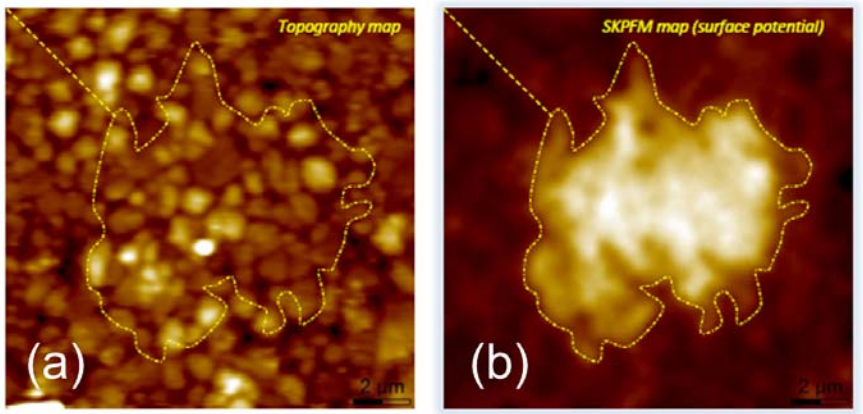

Fig. 10. AFM surface map (a) and corresponding map of surface potential (b) of the surface fragment of the graphene/Ni structure after vacuum annealing at 800°C for 5 min. The borders of the graphene flake determined from optical microscopy are superimposed on AFM and SKPFM images.

4. Conclusions

It was demonstrated that "sandwich" a-SiC/Ni multilayer structure can be used for synthesis of single-layer graphene flakes with the size more than 20 µm. RTA annealing in ambient nitrogen allow us to synthesize multilayer graphene with surface covering up to 80%. Close covering of the graphene layers of Ni grains results in surface asperity of the graphene layer and shift of the 2*D* Raman band to higher values. The SKPFM method is very sensitive for graphene layer indentification and extraction of the single-layer graphene flake size.

Acknowledgements

This work was supported by the National Academy of Sciences of Ukraine in the framework of the Ukrainian-

Russia project No. 39-02-13, the State Program of Ukraine "Nanotechnologies and Nanomaterials" through the Project #3.5.2.6/48 and SFFR Project F53/161-2013.

References

1. J. Hofrichter, B.N. Szafranek, M. Otto, T.J. Echtermeyer, M. Baus, A. Majerus, V. Geringer, M. Ramsteiner, and H. Kurz, Synthesis of graphene on silicon dioxide by a solid carbon source // *Nano Lett*., **10**, p. 36-42 (2010).
2. C. Berger, Z. Song, X. Li, X. Wu, N. Brown, C. Naud, D. Mayou, T. Li, J. Hass, A.N. Marchenkov, E.H.P.N. Conrad, First, and W.A. de Heer, Electronic confinement and coherence in patterned epitaxial graphene // *Science*, **312**, p. 1191-1196 (2006).
3. https://graphene-supermarket.com/CVD-Graphene-on-Metals
4. M. Nonnenmacher, M.P. O'Boyle, H.K. Wickramasinghe, Kelvin probe force microscopy // *Appl. Phys. Lett*., **58**, p. 2921-2924 (1991).
5. J Y. Wang, H. Wang, and G. Ma, Effects of high-temperature annealing on the structure of reactive sputtering a-SiC:H films // *Thin Solid Films*, **335**, p. 249-252 (1998).
6. A.C. Ferrari and J. Robertson, Interpretation of Raman spectra of disordered and amorphous carbon // *Phys. Rev. B*, **61**, p. 14095-14107 (2000).
7. A.V. Vasin, Sh. Muto, Yu. Ishikawa, A.V. Rusavsky, T. Kimura, V.S. Lysenko, and A.N. Nazarov, Comparative study of annealing and oxidation effects in a-SiC:H and a-SiC thin films deposited by radio-frequency magnetron sputtering // *Thin Solid Films*, **519**, p. 2218-2224 (2011).
8. L.M. Malard, M.A. Pimenta, G. Dresselhaus, and M.S. Dresselhaus, Raman spectroscopy in graphene // *Phys. Repts.*, **473**, p. 51-87 (2009).
9. A.C. Ferrari, J.C. Meyer, V. Scardaci, C. Casiraghi, M. Lazzeri, F. Mauri, S. Piscanec, D. Jiang, K.S. Novoselov, S. Roth, A.K. Geim, Raman spectrum of graphene and graphene layers // *Phys. Rev. B*, **97**, 187401 (2006).
10. E.H.M. Ferreira, M.V.O. Moutinho, F. Stavale, M.M. Lucchese, R.B. Capaz, C.A. Achete, and A. Jorio, Evolution of the Raman spectra from single-, few-, and many-layer graphene with increasing disorder // *Phys. Rev. B*, **82**, 125429 (2010).
11. D.S. Lee, C. Riedl, B. Krauss, K. von Klitzing, U. Starke, and J.H. Smet, Raman spectra of epitaxial graphene on SiC and of epitaxial graphene transferred to SiO_2 // *Nano Lett*., **8**, p. 4320-4328 (2008).
12. P. Poncharal, A. Ayari, T. Michel, and J.-L. Sauvajol, Raman spectra of misoriented bilayer graphene // *Phys. Rev. B*, **78**, 113407 (2008).
13. S. Latil, V. Meunier, and L. Henrard, Massless fermions in multilayer graphitic systems with misoriented layers: Ab initio calculations and experimental fingerprints // *Phys. Rev. B*, **76**, 201402 (2007).
14. K.S. Novoselov, A.K. Geim, S.V. Morozov, D. Jiang, Y. Zhang, S.V. Dubonos, I.V. Grigorieva, and A.A. Firsov, Electric field effect in atomically thin carbon films // *Science*, **306**, p. 666-669 (2004).